Stony Brook University

Stony Brook University

Novel adhesion properties of irreversibly adsorbed polymer chains

A Thesis Presented

by

Zhizhao Chen

to

The Graduate School

in Partial Fulfillment of the

Requirements

for the Degree of

Master of Science

in

Materials Science and Engineering

Stony Brook University

May 2016

Stony Brook University

The Graduate School

Zhizhao Chen

We, the thesis committee for the above candidate for the

Master of Science degree, hereby recommend

acceptance of this thesis.

Tadanori Koga – Thesis Advisor
Associate Professor, Department of Materials Science and Engineering

Jonathan Sokolov– Second Reader

Professor, Department of Materials Science and Engineering

Taejin Kim – Third Reader

Assistant Professor, Department of Materials Science and Engineering

This thesis is accepted by the Graduate School

Charles Taber
Dean of the Graduate School

Abstract of the Thesis

Novel adhesion properties of irreversibly adsorbed polymer chains

by

Zhizhao Chen

Master of Science

in

Materials Science and Engineering

Stony Brook University

2016

Abstract

Interpenetrations (or entanglements) between chemically identical polymers are important parameters in fundamental physics and industrial applications. However, little is known about the interaction between free polymer chains and chemically identical, but otherwise highly adsorbed chains on solid surfaces. Here we report an unusual interaction between free chains and chemically identical flattened chains which have many surface-segmental contacts with solids. Based on the mechanical adhesion measurements, we found the 2.5 nm-thick equilibrium polyethylene-oxide (PEO) flattened layer show no adhesion with the PEO melts even at $T > T_m$. Liquid contact angle measurements further revealed that the flattened layer has the same macroscopic surface tension compared to thin films. Hence, the unusual interaction between free chains and highly adsorbed flattened chains is not due to a difference in the surface tension, but is associated with the unique

chain conformation of flattened chains which cannot form sufficient entanglements with free chains in the melt. Since the formation of flattened chains is rather general, the presented experimental findings not only shed new light on the interfacial interaction between free chains and flattened chains near the solids, but also provide a simple and effective way to control and manipulate the adhesive properties and crystallization behaviors of thin polymer films prepared on solid surfaces. On the other hand, the "loosely adsorbed" polymer chains, which are formed as a result of limited adsorption space on the solid surface, do display a degree of adhesion with the bulk polymer. We postulate that the loosely adsorbed chains act as "connectors" which promote adhesion effectively across the solid-polymer interface, while the "flattened" chains are so densely compact on the substrate that the outer free chains cannot penetrate into it to form adhesion.

Table of Contents

List of Figures

List of Tables

List of Schemes

List of Abbreviations

PEO: poly(ethelene oxide)

PS: poly(styrene)

AFM: Atomic Force Microscopy

Acknowledgments

Firstly, I would like to express my deepest appreciation to my thesis advisor, Tadanori Koga, for his unending mentorship and guidance, helping me to hone and enhance my skills as a master's student. His sagacity as my teacher helped make this research and thesis possible. Throughout my research in the lab, he has imbued me with tremendous knowledge and understanding of polymer science which I will be sure to carry with me in my future endeavors.

My thanks also goes out to Mani Kuntal Sen, Deborah Barkley, Justin Cheung, Naisheng Jiang, Jiaxun Wang, Wenduo Zeng, all lab mates in Professor Koga's group, who supported and helped me copiously during my time as a master's student.

A heartfelt thanks to my parents, Jingrui Chen and Shunbing Yang, for their inexorable patience and gracious support of my master's studies as well as their infinite consideration of my wellbeing at Stony Brook University.

Chapter 1 Introduction

1.1 What do we know about adsorbed nanolayers?

A. General background. A spin-coating process is a well-established technique to prepare homogenous polymer thin films on planar solids. But, it is known that this rapid solvent evaporation process results in non-equilibrium stressed conformations of polymer chains on solids and such residual stress causes film instability[4-6] and changes in properties of polymer thin films[7, 8]. In order to eliminate the residual stress, prolonged thermal annealing (at temperatures far above T_g) is typically required[6, 7, 9]. Aside from equilibration, it is also evidenced that such thermal annealing expedites polymer adsorption onto even weakly attractive solids[10, 11] . This can be explained by the fact that the total enthalpic gain due to an increase in the number of surface-segmental contacts overcomes a loss in the conformational entropy of the chain during the transition from a randomly coiled state to an adsorbed state[11, 12]. Guiselin[13] proposed the experimental procedure to unveil the irreversibly adsorbed polymer layer (so-called "Guiselin brushes" composed of a mixture of tail and loop segment sequences[11, 14]): One has to equilibrate the melt or dense solution against a solid surface; The unadsorbed chains can then be removed by a good solvent, while the adsorbed chains are assumed to maintain the same conformation due to the irreversible freezing they experience through many physical solid-segment contacts. Despite experimental difficulties, several research groups have already demonstrated that Guiselin's approach is practical for various homopolymers, revealing the presence of the adsorbed nanolayers onto planar surfaces[10, 15-25]. The formation of the adsorbed nanolayer has been reported on various nanoparticle surfaces as well[26-33]. Interestingly, Kumar and co-workers have shown that the adsorbed nanolayer can be significantly thinner around nanoparticles than at chemically similar planar solid surfaces[32]. Very recently, the PI and co-workers found that the adsorbed polybutadiene (PB) nanolayer on carbon black filler surfaces swells in a good solvent, displaying a parabolic profile with a diffuse tail[34]. Furthermore, the neutron spin echo results indicated the collective dynamics of the swollen chains that can be explained by the so-called "breathing mode"[35].

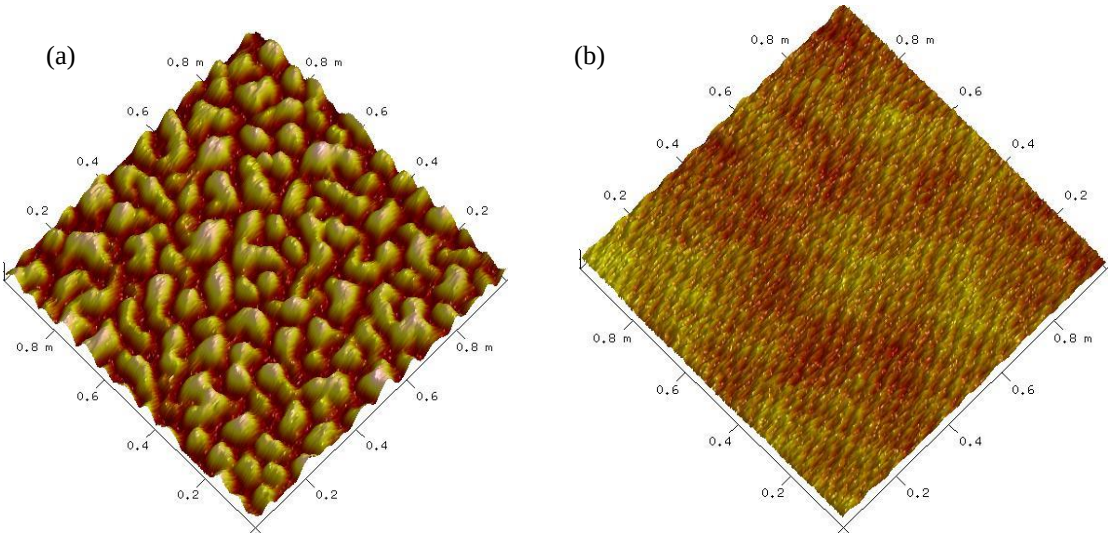

Figure 1. AFM height images of (a) the PS (M_w = 290 kDa) flattened layer surface and (b) interfacial sublayer surface at t_{an} = 100 h. The scan sizes and height scales of the images are 1 μm × 1 μm and 0 - 6 nm, respectively[24].

B. Nanoscale structures of the two different adsorbed chains. Here we briefly explain our recent experimental findings in the structures and the formation process of the adsorbed nanolayers. The details have been described in our recent book chapter[36]. We used PS as a model system and prepared the adsorbed nanolayers on Si substrates using Guiselin's approach. Si wafers were pre-cleaned using a hot piranha solution for 30 min, and were subsequently rinsed with deionized water thoroughly. We confirmed that the native oxide (SiO_x) layer after the piranha solution cleaning had a thickness of 2.4 nm on the Si (hereafter assigned as "non-treated Si"). The water contact angle of the non-treated Si (just before spin-coating of polymer films) was estimated to be less than 10 º. In order to change the surface attraction of the polymer, the non-treated Si wafers were further immersed in an aqueous solution of hydrogen fluoride (HF) for 20 s to remove the SiO_x layer (hereafter assigned as "HF-etched Si"). It should be noted that a thin SiO_x layer of 1.3 nm in thickness was, however, reproduced even immediately after HF etching, possibly due to atmospheric oxygen and moisture[25, 37]. The water contact angle of the HF-etched Si was determined to be 80 ± 1 º. Hence, the HF-etched Si has a very different hydrophobicity when compared to the non-treated Si. Spin-cast PS films (≈ 50 nm in thickness) prepared on the HF-etched Si substrates were first annealed at 150 ℃ for a long period of time (up to 200 h) and then solvent leached with toluene at room temperature repeatedly until the thickness of the residual layer remained unchanged. The final residual layers (i.e., the adsorbed nanolayers) were further

dried under vacuum at 150 ℃ to remove any excess solvent trapped in the films. X-ray reflectivity (XR) in conjunction with a Fourier transformation method, a powerful tool to evaluate detailed structures for low x-ray contrast polymer multilayers[38-40], was used to obtain important data related to the details of the film structures.

The XR results intriguingly showed that the adsorbed nanolayers ($M_w \geq 123$kDa) are composed of two distinct density regions in the direction normal to the film surface: the inner higher-density region (~ 10 % higher than the bulk) composed of the flattened chains with about 2 nm in thickness regardless of M_w and the outer bulk-like density region whose thickness increases with increasing M_w[24, 25, 36, 41] (see, Fig. 2). The insensitivity of the thickness of the inner flattened chains to M_w can be drawn by a counterbalance between the conformational entropy of the chains and the energy gain of the attached segments to the surface in the total free energy[12, 24]. The formation of the flattened layer on a planar substrate is also consistent with the Brownian dynamic simulation results[42]: flexible homopolymer chains tend to orient their conformations parallel to the surface and form a compact, higher density layer relative to the bulk in equilibrium. Furthermore, we found that solvent leaching with chloroform (a better solvent than toluene for PS) allows for

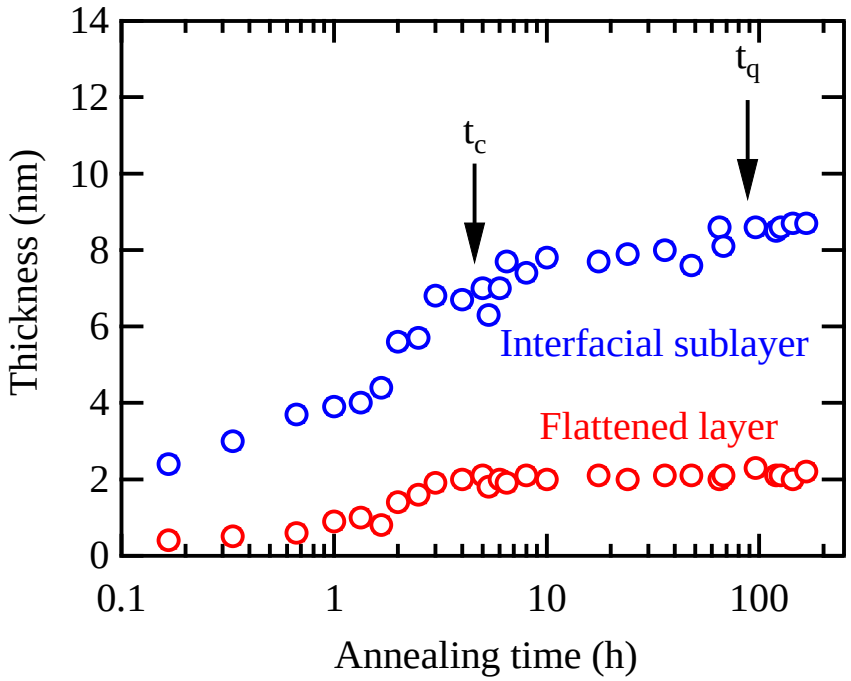

Figure 2. Growth curves of the PS (M_w = 290 kDa) interfacial sublayer (blue circles) and flattened layer (red circles) against t_{an} at 150 ℃ measured by XR[24]. The crossover time (t_c) from the power-law growth to logarithmic growth for the interfacial sublayer is indicated by the left arrow. The final adsorption time to reach a plateau (i.e., the quasiequilibrium state) in the growth curve is indicated as t_q.

the unveiling of the lone inner high-density region[25]. This selective extraction of the two adsorbed layers is attributed to the large difference in desorption energy between the outer loosely adsorbed chains and the inner flattened chains, which is proportional to the number of segment-surface contacts[43, 44]. Hereafter, we assign the adsorbed nanolayer composed of the inner flattened chains and outer loosely adsorbed chains as an "interfacial sublayer", while the adsorbed nanolayer composed of the lone flattened chains is assigned as a "flattened layer"[25], unless otherwise stated.

Fig. 1 shows representative surface morphologies of (a) the PS flattened layer and (b) the PS interfacial sublayer after achieving the "quasiequilibrium" state (i.e., the final adsorbed layers whose thickness remains unchanged against annealing time (t_{an}) at $t_{an} > t_q$, as shown in Fig. 2). From the figure we can see that the flattened layer has microscopic "textures" with a characteristic length of about 100 nm, while the surface of the interfacial sublayer is homogeneous. It is hence reasonable to suppose that the empty regions of the flattened layer correspond to the sites where the loosely adsorbed chains grew and were then removed by the chloroform leaching. In addition, as summarized in Fig. 2, the two different chain architectures emerge and grow independently on the solid surface[25], while the time scale for the initial nucleation and growth of the flattened chains is predicted to be only a few hundred nanoseconds[42, 45]. We have also revealed that this two-layer formation is general regardless of the choice of polymers with respect to varying surface-segment interactions and intramolecular architectures[25, 46]. Furthermore, it was found that the surface coverage of the quasiequilibrium flattened layer increases with increasing the magnitude of solid-segment interactions: the surface coverage follows poly(2-vinylpyridine) (P2VP) > poly(methyl methacrylate) (PMMA) > PS with the nearly same M_w on the same substrate[25].

C. Roles of the adsorbed nanolayers in film stability. We recently found that the two different adsorbed polymer chains play opposite roles in thermal stability of supported single PS thin films[41]. PS spin-cast films (20 nm in thickness) with eight different molecular weights prepared on non-treated Si and HF-etched Si substrates were used as a model. We used the exact same protocols for all Si wafer cleaning to avoid possible differences in the surface chemistry of the oxide layer that affects dewetting behavior of thin PS films[47]. The samples were annealed at 150 ℃ $> T_g$ (≈ 100 ºC) for prolonged times under vacuum and subsequently quenched to room temperature. This rapid quench allowed us to preserve the film structures via vitrification of the

polymer and to further measure the film surfaces by using optical microscopy (OM) and atomic force microscopy (AFM) at room temperature.

The OM experiments clearly showed that all the PS thin films with $M_w \leq 50$ kDa broke up into droplet-based cellular patterns (i.e., dewetting), while no signs of dewetting were observed for $M_w \geq 123$kDa. We further confirmed that the PS films with $M_w \geq 123$kDa remained stable at least for

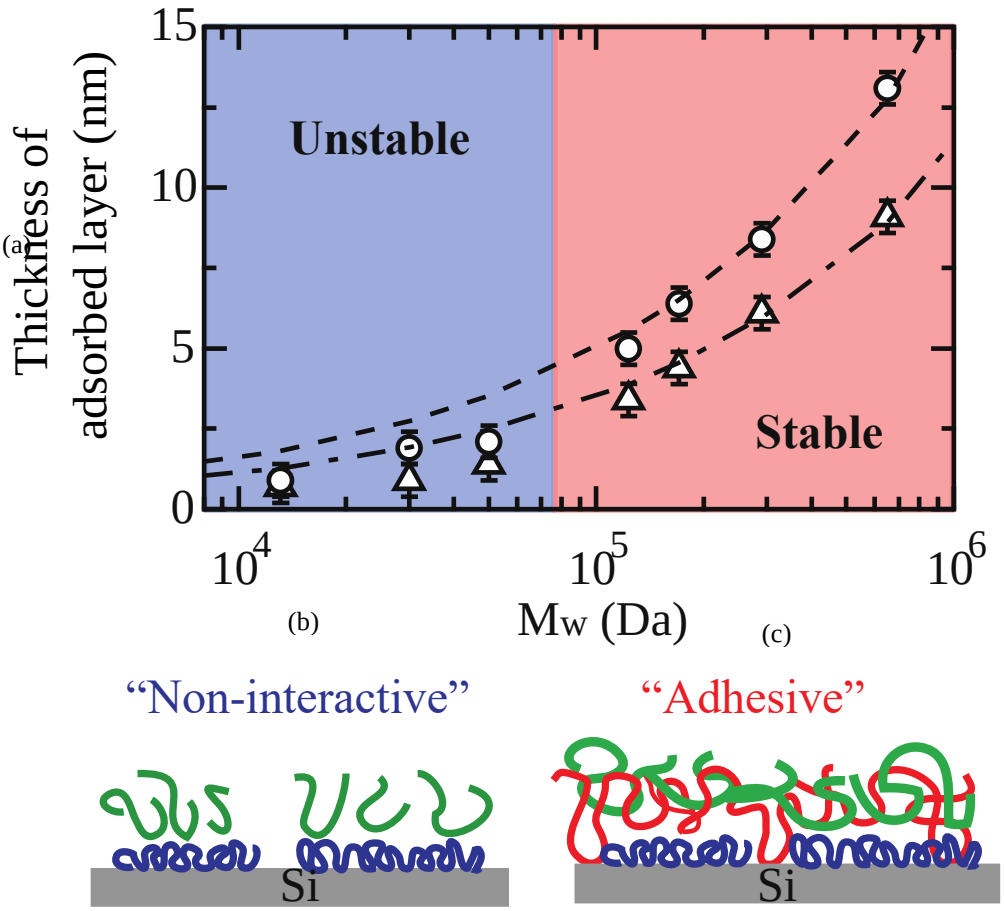

Figure 3. Thicknesses of the residue PS layers (h_{ads}) on the HF-etched Si (circles) and non-treated Si (triangles) as a function of M_w after leaching with toluene. The dotted line and dotted-solid line correspond to the relationship of $h_{ads} = 0.65\ R_g$ for the HF-etched Si and $h_{ads} = 0.46\ R_g$ for the non-treated Si. The PS thin films show the *M*w dependence of the macroscopic film stability, as indicated in the different colors. Schematic views of the chain conformations in the unstable (Fig. 3b) and stable regions (Fig. 3c). The green chains correspond to free polymer chains in the matrix of the film. The data are from Ref. 41.

6 weeks at 150 ℃. Similar M_w dependence was observed for the 20 nm-thick PS films on the non-

treated Si[41]. Hence, the visual observation evidenced a macroscopic dewetting-to-wetting transition controlled by M_w, as reported previously[48, 49]. At the same time, the AFM height image of the dewetted region revealed the formation of "nano-textures" with a characteristic length of about 50 nm (data not shown), which is similar to previous experimental findings[50, 51]. Hence, it is suggestive that the instability of the low M_w PS thin films takes place at the adsorbed polymer-free polymer interface, which is analogous to "autophobicity" where polymer melts in contact with a chemically identical polymer brush are unstable[52-58].

In order to explore a correlation between the film stability and the interfacial conformations, we rinsed all the annealed PS films with toluene thoroughly at room temperature. The residual films after post-annealing at 150 ℃ under vacuum were then characterized by AFM and XR. Fig. 3a summarizes the thicknesses of the residue layers (h_{ads}) as a function of M_w of the PS thin films. We found that the PS residue layers composed of $M_w \geq 123$ kDa show the two-layer structures (i.e., the interfacial sublayers, see Fig.3c) regardless of a choice of the Si substrates. The total thicknesses have the relationship of $h_{ads} = 0.65\ R_g$ for the HF-etched Si and $h_{ads} = 0.46\ R_g$ for the non-treated Si (Fig. 3a), both of which are in agreement with previous results on the PS adsorbed nanolayers[10, 24, 59]. On the other hand, Fig. 3a shows a clear failure of the scaling laws for the residual PS films with $M_w \leq 50$ kDa. We found that the residue layers with $M_w \leq 50$ kDa showed nano-textures and the total thicknesses were about or less than 2 nm, proving that the residue layers are the flattened layers. Hence, the correlation between the interfacial chain architectures and film stability can be drawn: the PS films are stable when the loosely adsorbed polymer chains are formed on the substrates (Fig. 3c); conversely, the lone flattened chains are non-interactive even with chemically identical free polymer chains and will result in autophobic dewetting (Fig. 3b). To validate the interfacial roles of the two different adsorbed chains, we further mimicked the single PS layer by utilizing split layers composed of a PS overlayer on top of the PS flattened layer or the interfacial layer, while the total thickness of the split layers was fixed to 20 nm. As a result, we found that the low M_w ($M_w \leq 50$ kDa) PS overlayers always dewet on the flattened layer under the same annealing conditions used for the single PS layer experiments, while the high ($M_w \geq$ 123kDa) PS overlayers appear to be stable on the interfacial sublayer, both of which support the single layer data shown in Fig. 3a.

1.2 Adhesion between polymers

Polymer adhesion is very important for its general use in the processes of welding, lamination of composites, polymer processing, and polymer blending, and have been widely studied for years. Numerical theories have been developed to explain the polymer behavior during adhesion process. However, it still remains unclear for the complexity of polymer.

Polymer self-adhesion, which means adhesion between the same polymers, is normally studied by the polymer adhesion experiment[1, 60]. In the experiment, two pieces of polymer thin film are brought into contact and annealed at a temperature higher than its T_g to induce the diffusion across the interface between these two polymer films (Figure 4). During this process, a zone of two polymer films overlapping with each other is formed and boarded, while the strength of the interface is enhanced with time as well and ultimately reaches equilibrium.

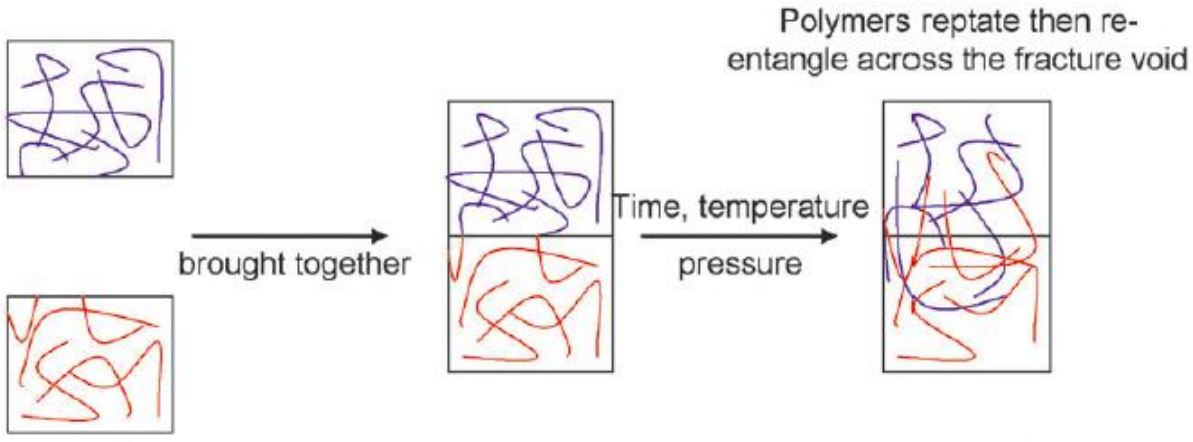

Figure 4. Schematic image for the adhesion between polymer thin films[3].

Interdiffusion of the chains across the interface can be mainly explained by the reptation model[61], which is in good agreement with many experiment results[62-65]. In this model, it's assumed that the polymer chains can only move alone their contour length because mobility in other direction are constrained by the entanglement with other chains surrounding them. Thus, significant diffusion happens first at the end of the chain and then the central part of the chain follows. Basically the interdiffusion process can be divided into several steps (Figure 5). In the first stage (diffusion time t<entanglement time t_e), chains diffusion across the interface happens

rapidly with most of the diffusion being caused by the Rouse-like motion of the polymer chain segments within the tube. This process starts and saturates in a short time because of the entanglement restriction to the chain motion. In this stage, the increase of adhesion strength is very small because Rouse-like motion does not produce chain entanglement. After t_e, the motion normal to the virtual tube starts to constrain by the entanglement and become much slower. Later, between the rouse time t_R and reptation time t_{rep}, since the tube itself is a random path, the chain sections are retarded in their excursion and chains start to diffuse out of the origin tube. And finally, after t_{rep}, the interface has disappeared and motion of chains is dominated by normal Fickian diffusion. The reptation time can be scaled to

$$t_{rep} \sim L_t^2 / D_{tube} \tag{1}$$

In which L_t is the tube length and D_{tube} is the tube diffusion coefficient.

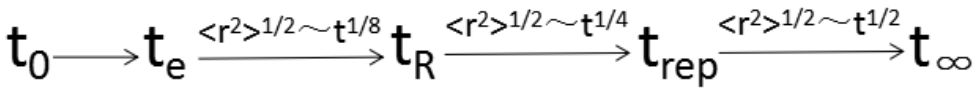

Figure 5. Illustration of the relationship between average displacements of the chain segments ($<r^2>^{1/2}$) and diffusion time (t) in reptation theory.

While the time dependence of interdiffusion for the chains across the interface can be reasonably explained by the reptation theory, the exactly arrangement of chains at the interface that cause the resistance to fracture is still unclear. Figure 6 shows several hypotheses to explain the arrangement of chains that control mechanical strength at adhesion interface[66-69]. Nevertheless, all these hypotheses agree that adhesion between polymers is controlled by both the chain coupling across the interface and energy dissipation processes in the material.

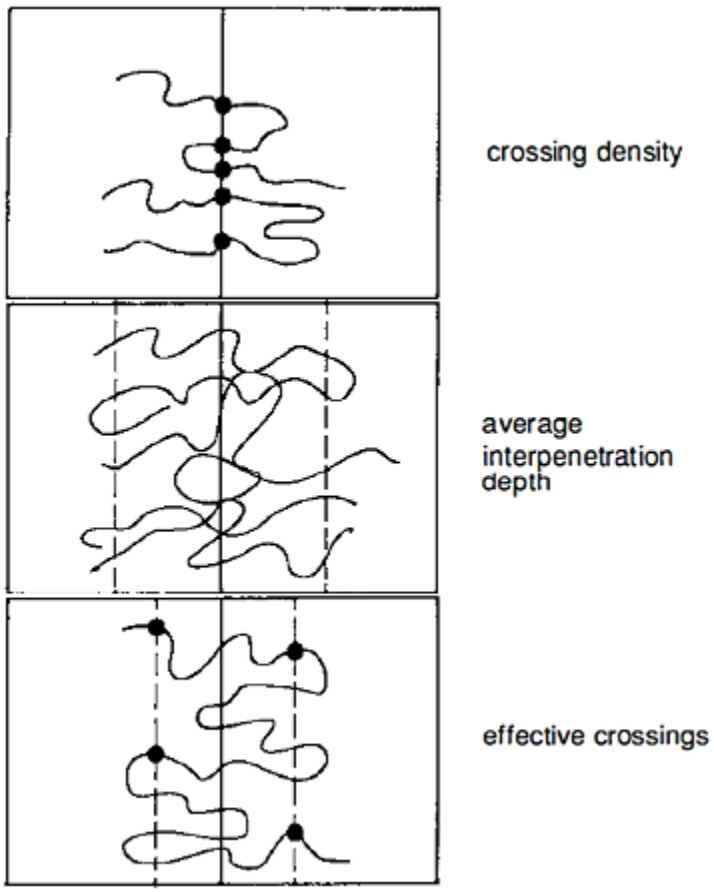

Figure 6. Several hypotheses for arrangement of chains that control mechanical strength at adhesion interface[1].

Besides, it's proved that diffusion for the chain ends is much faster than that for the central part[70].

1.3 Fracture between polymers with interfacial entanglement

Characterization for the fracture between polymers with interfacial entanglement provides a method to investigate the adhesion process we discussed above. Thus, by using a range of techniques on various systems, researches have done lots of work on the evolution of interfacial

strength with interdiffusion time and interdiffusion width and its connection to interfacial structure[2, 71-75].

Before further discussing the relationship between the interfacial strength and its influencing factors, one should be noted is the failure mechanism for the interfacial fracture. Studies show that when the interface is able to sustain a stress which is higher than the crazing stress of the homopolymer, there is a transition in failure mechanism from chain pull-out to crazing[71, 76]. The critical stress for the formation of a craze σ_{craze} can be expressed as a function of the areal density of the copolymer chains Σ, the degree of polymerization N, and the static monomer friction coefficient of the block being extracted f_{mono}. As shown in figure 7, if the areal density of copolymer chains Σ is not too high, the transition point can be expressed by:

$$f_{mono}\, N\, \Sigma > \sigma_{craze}$$

When the situation is satisfied, the failure mechanism is controlled by crazing. The formation of this zone causes a change in regime of the fracture toughness dependence with Σ, from $G_c \propto \Sigma$ to $G_c \propto \Sigma^2$.

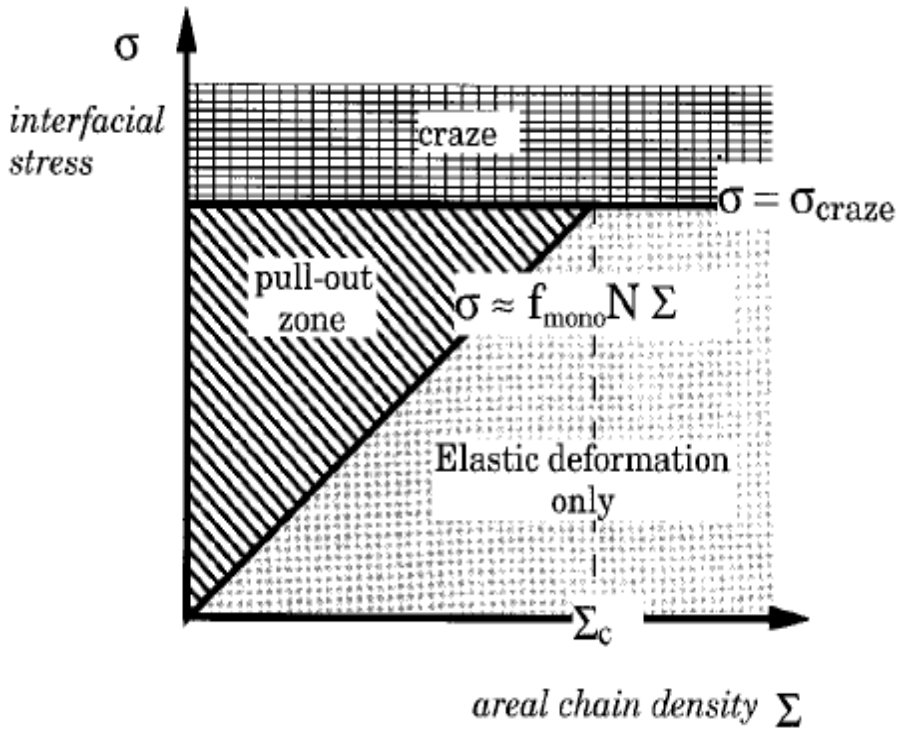

Figure 7. Schematics of the interfacial stress as a function of the areal density of connecting chains. For low areal density of chains the failure of the interface, when the interfacial stress is increased, occurs by chain pullout. For areal densities higher than ₵, the failure is preceded by the formation of a plastic zone.

By changing the annealing temperature, polymer molecule weight, or the bromine concentration in the polymer, Schnell et al[2, 72]are able to obtain different interfacial width without changing the mechanical properties of the bulk polymers so that they can directly study the relationship between interfacial width and adhesion strength.

1.4 Polymer diffusion near attractive solid substrate

Polymer chains near solid substrate shows different diffusion property compared with the chains in the bulk polymer because of the confinement and the interaction between the polymer chains and the substrate.

Experiments indicate that the mobility of polymer chains, which is usually characterized by the diffusion coefficient, significantly decrease when it close to a solid surface. B. Frank al et[77] report

that there is a significant decrease in the diffusion coefficient even when the distance from the substrate is more than $25R_g$, while the polymer chains can easily assume undistorted and unperturbed configuration at such a film thickness.

Polymer interdiffusion near an attractive solid substrate is studied by E. Lin and other co-researchers by constructing a bilayer system[78]. They found that thickness of the lower polymer film strongly influent the interdiffusion. When the thickness of lower film is lower than $2R_g$, the effective diffusion constant is 2 orders of magnitude smaller than that of the bulk polymer. The effective diffusion constant recover until the thickness the more than $7R_g$ (Figure 8). Though limited evidence existed at that time, in their analysis they have pointed out that the mobility change is caused by the chain conformations at the interface. When the thickness is less than R_g, the conformations being distorted parallel to the substrate and the numerous contacts per chain with the attractive surface significantly reduce the mobility of polymer chains. On the other hand, for films between 1 and 2 R_g thick, the entanglement between the polymer chains near the polymer-polymer interface and the adsorbed chains near the substrate become the main reason that the mobility reduction. Thus, its mobility shows a regularity that higher than that of the thinnest one but lower than that of the thicker one.

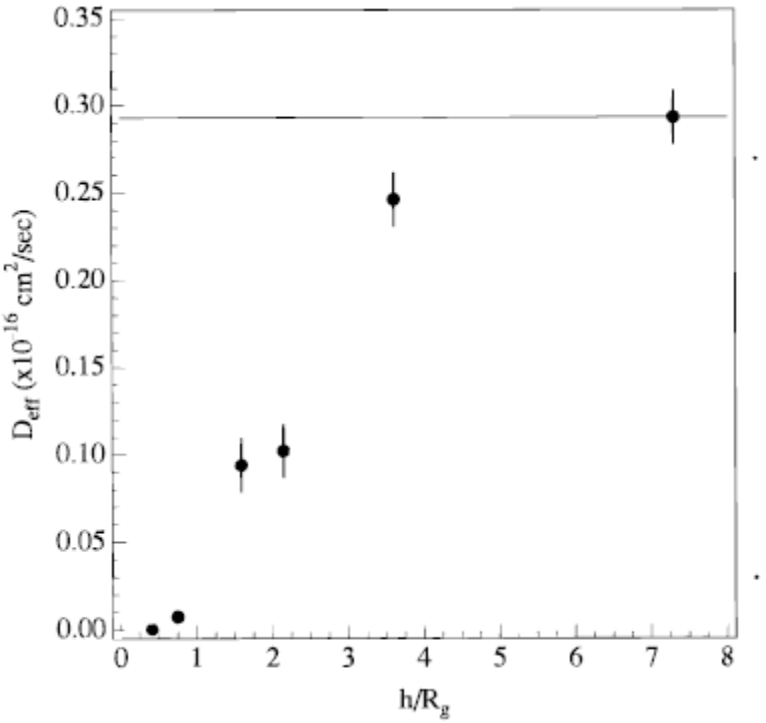

Figure 8. Relationship between effective diffusion coefficient (D_{eff}) and the thickness of lower film for the PMMA bilayer system.

X. Zheng et al.[79, 80] also show that the diffusion coefficient of polymer chains decrease rapidly with the distance between the polymer chain and the substrate. Besides, they provided a unique method to explore the relationship between the structure and the diffusion property of polymer film, proving that the rate of diffusion strongly depends on the mixing of polymer within the matrix.

1.5. Hypotheses

The aforementioned effect of the loosely adsorbed chains on the film stabilization can be explained by the concept of "connector molecules"[81] which promote adhesion and transmit the stress effectively through the (adsorbed) polymer- (free) polymer interface. Raphaël and de Gennes considered a smooth solid surface on which long polymer chains are tethered at sufficiently low grafting density[81] so that the chains do not overlap with each other[82]. If the solid surface grafted with the polymer chains is put into together with a polymer melt composed of the same polymer, the grafted chains tend to interpenetrate into the bulk polymer so as to recover their equilibrium Gaussian conformation and gain entropy. When one pulls out the polymer melt in the direction

normal to the surface (Fig. 9a), the connector chains become fully stretched inside the gap between the polymer melt and solid surface, as shown in Fig. 9b. This additional energy can be considered as the work of the force necessary to extract one connector molecule from the bulk over the length of the extracted connector multiplied by the number of the connectors per the unit area. The enhancement of adhesion energy compared with the thermodynamic work of adhesion is thus directly indicative of the degree of interdigitation of the connectors into the bulk polymer.

However, the molecular-scale descriptions of the adhesion enhancement/reduction associated with the two different adsorbed chains (see, Fig. 9b&c) are currently lacking. As mentioned above, the adsorbed chains are mainly composed of loops and tails[55, 58], which make the situation more complicated than end-grafted chains. For instance, according to Leger and Creton[83], it is expected that the connector chains composed of lone end-grafted polymers (tails) need to be longer than the entanglement length to start promoting adhesion. However, as shown in Fig. 9, the length of the connector composed of the loosely adsorbed chains is much shorter (~ 4 nm) than the entangled length of PS (~ 9 nm)[84]. Therefore, we propose to mimic the interface shown in Fig. 9 by preparing bilayers of a PS bulk overlayer on top of the flattened layer or interfacial sublayer and quantify the adhesion force of the two different adsorbed chains experimentally.

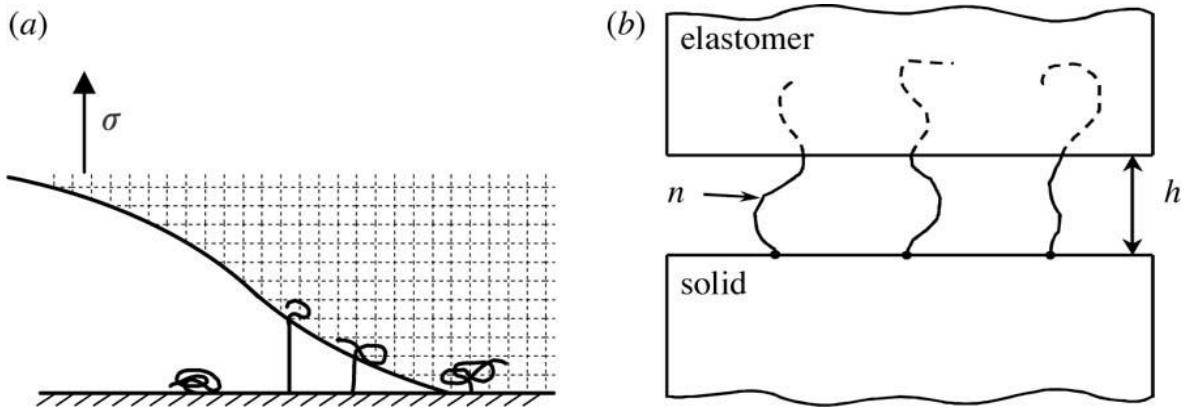

Figure 9. Schematic illustrations of opening of a fracture between a cross-linked polymer and a solid surface on which polymer chains are end-grafted[92]: (a) opening process with connector chains being progressively extracted from the elastomer, and then lying flat on the solid surface and (b) expanded view near the opening zone. Each chain has *n* monomers exposed to air in the gap. Van der Waals interactions between monomers are strong enough to maintain the connector stretched when one tries to separate the two partners of the assembly.

Chapter 2 Experimental

2.1 Sample Preparation

Poly (ethelyne oxide) (PEO) (Average M_n=20kDa, Sigma-Aldrich, product no. 81300) and four different polystyrene (PS) (Average M_n=50kDa, 100kDa, 221kDa and 650kDa, M_w/M_n<1.15, Pressure Chemical Co. and Scientific Polymer Product Inc.) were used. We hereby denote them as 20kPEO, 50kPS, 100kPS, 221kPS and 650kPS, respectively. The Si wafers were pre-cleaned by a 1:1:1 mixture of ammonium hydroxide, hydrogen peroxide and water for 15~30 minutes at 125~140 ℃, and then further cleaned by immersion in a hot piranha solution (i.e., a mixture of H_2SO_4 and H_2O_2 [Caution: A piranha solution is highly corrosive upon contact with skin or eyes and is an explosion hazard when mixed with organic chemicals/materials; extreme care should be taken when handing it]) for 30 minutes at 125~140 ℃. The Si wafers were then washed with deionized water for several times after each step to fully erase the residual liquid used. After that, the native oxide layer on the Si substrates was removed by dipping the substrates into an aqueous solution of hydrogen fluoride (HF) for 15 s. From X-ray reflectivity characterization, a thin SiO_x layer of 1.3nm-thick was found on the substrate even right after the HF etching. In this study, all Si substrates are HF-passivated to ensure stronger interactivity between the polymer and Si substrate.

PEO and PS thin films with different thicknesses were prepared on the substrates via spin coating. The rotation time was fixed to 30 seconds and the rotation speed was 2500 rpm. The thickness of thin films was characterized by ellipsometry technique (Rudolf Auto EL- II), with a refractive index of 1.455 for PEO and 1.589 for PS, respectively.

To produce the PEO and PS interfacial layer and flattened layer, 50 nm-thick PEO and PS spin-cast films were prepared and then annealed at the temperature far above their glass temperatures (T_g=85 ℃ for PEO and T_g=190 ℃ for PS) under vacuum below 10^{-3} Torr for several days. These films were then leached in baths of a fresh good solvent (chloroform for PS flattened layer, chlorobeneze for PEO flattened layer, and toluene for both PS interfacial layer and PEO interfacial layer) at room temperature until the resultant film thickness remained unchanged. Solvents with different desorption energy were used to obtain the adsorbed layers with different thickness. The

resultant interfacial layers were post-annealed at temperature above T_g in vacuum oven overnight to remove any excess solvent molecules trapped in the films.

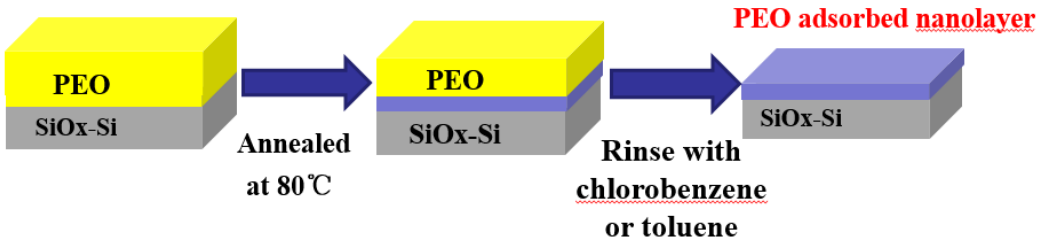

Scheme 1. Sample preparation process used in experiment

2.2 Custom-built adhesion testing device

The resistance to fracture for the two polymer layers were characterized by a custom-built adhesion testing device based on the principle of Hooke's Law[85]. Scheme 2.(a) shows a photo of the instrument. The PEO spin-coated thin films or the adsorbed layers prepared on the HF-Si substrates (1 cm ×1 cm in surface area) were first pressed together with an upper "bulk" (approximately 200 nm-thick) PEO film on the HF-Si substrate with a constant pressure of 16 kPa at high temperatures. The bottom very thin spin-coated thin films or adsorbed layers were then fixed to an experimental stage with glue (Loctite Super Glue, Henkel Corporation), while the upper bulk film was attached to one end of a mechanical spring with a spring constant (k) ranging from 4 N/cm with the same glue. The spring was chosen so as to limit the maximum displacement up to 1 cm, preventing the breakage of the spring and at the same time allowing us to reproduce the experimental data. Note that the adhesive strength of the glue is much stronger than that of the polymer/polymer interface. After a given pressing time was attained, the spring was gradually pulled out until the two attached films were separated each other, as shown in Scheme 2.(b). The critical normal force was then estimated from the maximum displacement of the spring via the Hooke's Law. The fracture stress can be then calculated as the fracture force divided by the surface area of the film (1 cm^2). In this

study at least 5 measurements were made for each polymer par, and the experimental uncertainty was taken as the standard deviation of all measurements.

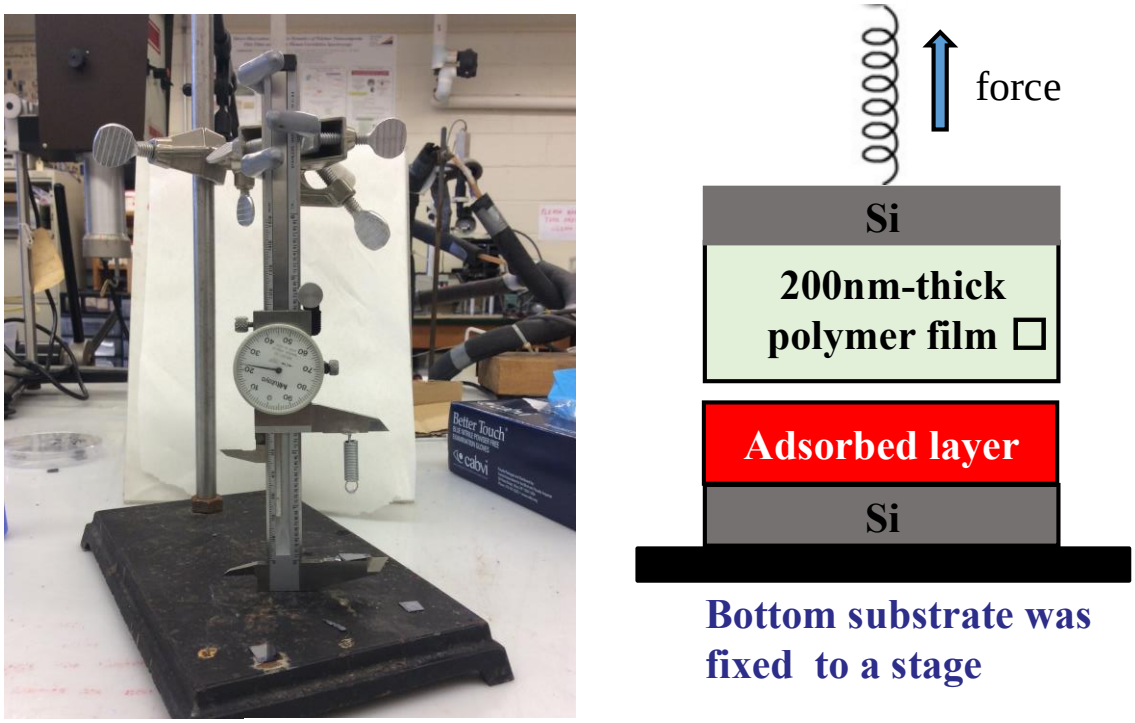

(a) (b)

Scheme 2. Device setup and experiment procedure

2.3 Ellipsometry Measurement

The thickness of polymer thin film is measured by an ellipsometer (Rudolf Auto EL- II), the reflective index (NU) for PEO film and PS film is 1.455 and 1.589, respectively. Besides, for the substrate, its reflective index (NS) is 3.858 and its extinction coefficient (KS) is 0.018.

Figure 10. Ellipsometer

2.4 Atomic Force Microscope (AFM) measurements

Atomic force microscope (AFM) (Digital Nanoscope III) was used to further study the surface morphology of PEO or PS thin films. A standard tapping mode was conducted in air using a cantilever with a spring constant of approximately 40N/m and a resonant frequency of 332 kHz. The scanning density was 256 or 512 lines per frame and the scan rate was 1.0 Hz.

Chapter 3 Results and discussion

3.1 Optimization of experimental parameters

Generally, the critical normal stress is mainly determined by the properties of polymer chain (including its intrinsic properties and chain conformation), pressing force, annealing temperature, and annealing time.

In order to make sure that the adhesive strength between the two polymer layers has reached in equilibrium, optimized experiments were performed with varying pressing time at the constant temperature of 85 °C, which is higher than the bulk melting temperature. As shown in Fig. 11, the time dependence of the fracture strength for PEO (M_n=20kDa) were characterized.[86]

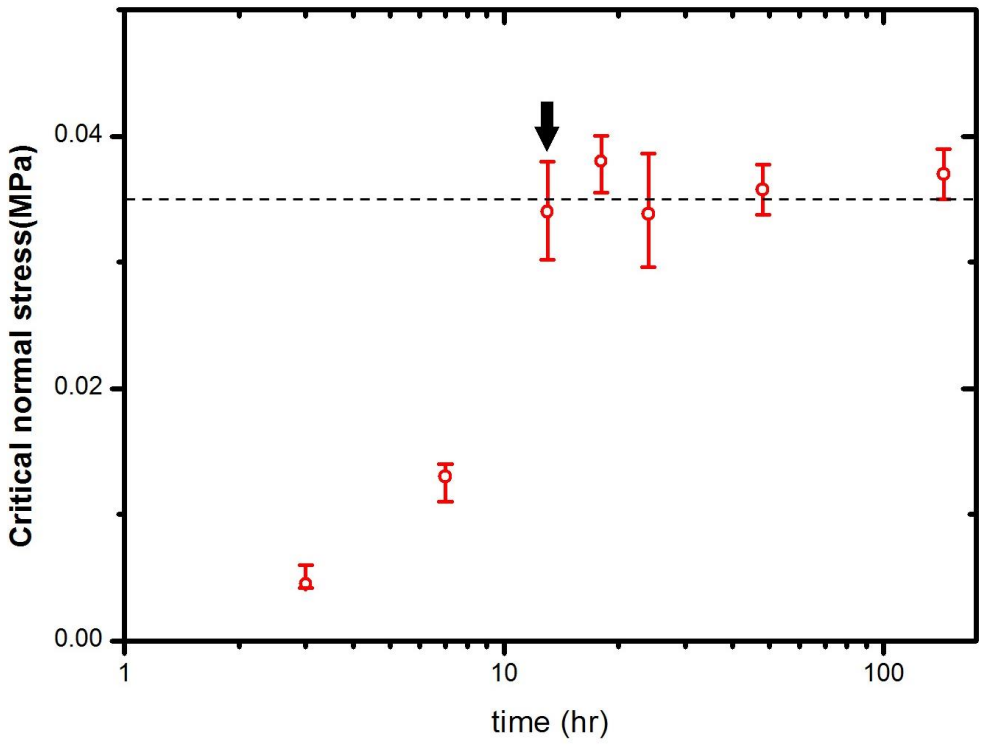

Figure 11. Adhesion strength dependence of adhesion time for 20 kDa PEO spin cast thin film with thickness of 8 nm under 85 °C. The equilibrium time is indicated in the arrow.

As we can see, the adhesion strength increase at first and then reaches a plateau after 13 hours and adhesion strength remain stable after that.

It should be noted that the equilibrium time for this system (13 hours) is much longer than that of the PEO reptation time in bulk polymer[87], indicating its mobility is much lower than the chains in the bulk. As we discussed in the introduction part, it has been proved that the mobility of polymer chains near a substrate is much lower than that of the bulk polymer chains. Since the thickness of bottom PEO thin film here only equals nearly $2R_g$, it's reasonable to explain the long equilibrium time by the fact that near a free surface (Si substrate), the mobility of PEO chains are perturbed.

3.2 Thickness dependence of fracture strength

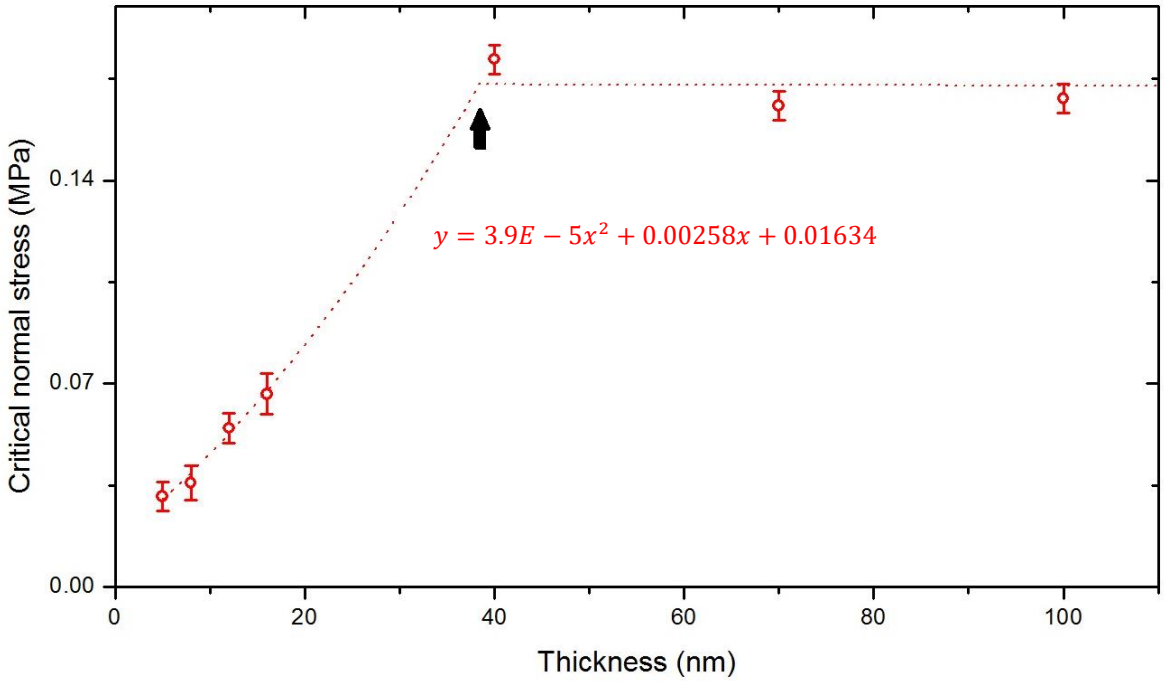

Figure 12. Adhesion strength dependence with the thickness of bottom layer. The fitting parabolic equation is shown in the figure and the critical thickness is indicated by the arrow.

We first characterized the instrument by using spin-cast PEO thin films. Fig. 12 shows the adhesion strength of the bilayers composed of the top 200 nm thick film and bottom spin-cast thin films with thickness ranging from 5 to 100 nm for the 20kDa. Note that the molecular weights are larger than a critical threshold ($6M_e$, M_e: the entanglement molecular weight. For PEO[88], M_e = 1780

so that the fracture is expected to takes place via cracking[89]). As seen in the figure, the normal stress can be fit with a parabolic function as a function of the thickness of the bottom spin-cast films when the thickness is thinner than 40 nm. It should be noted that this parabolic behavior correspond well with theoretical predictions. When $M_w > M_c$, the interfacial adhesion is mainly controlled by entanglements of polymer chains[90]. As a crack is propagated at the interface, entangled chains are broken. According to the scaling analysis of adhesion between immiscible polymers[89], the resistance to fracture (or the interfacial adhesion, G_c) is correlated to the characteristic number of interfacial entanglements (N_{ent}) via $G_c \propto N_{ent}^2$. In addition, Ge and co-workers[91] reported that N_{ent} scales linearly with the interfacial width *(w_I)* for miscible polymer systems. Hence, the scaling of $G_c \propto \boldsymbol{w_I^2}$ is expected. Previously, by using neutron reflectivity (NR), Li and co-workers[78] demonstrated that there is almost no interdiffusion between a bottom deuterated poly(methyl methacrylate) (PMMA) with $0.38R_g$ thick and a hydrogenated PMMA overlayer and the interfacial width was only 2 nm even after several hours of annealing at 150 ℃ >> T_g. In addition, they showed that the interfacial width increased with increasing the thickness of the bottom d-PMMA thin films (ranging from 0.38Rg to 3.6Rg) at given times, which are far beyond the bulk reptation time. This limited interdiffusion would be attributed to strong chain pinning to the substrate surface, as the film thickness becomes thinner[78, 92]. Hence, it is reasonable to suppose that similar suppressed interpenetration takes place in the present case (i.e., the given scaled film thickness of the bottom PEO layers ranging from R_g to $3.0R_g$), resulting in a similar tendency of the thickness dependence of the interfacial width. We postulate that this leads to the observed parabolic correlation between G_c and w_I. Further studies using NR are needed to quantify the interfacial width for the present system. On the other hand, when the thickness of bottom layer is higher than 40 nm, the normal stress become stable. Similar results have been reported by other groups[2, 72, 93](Figure 13).

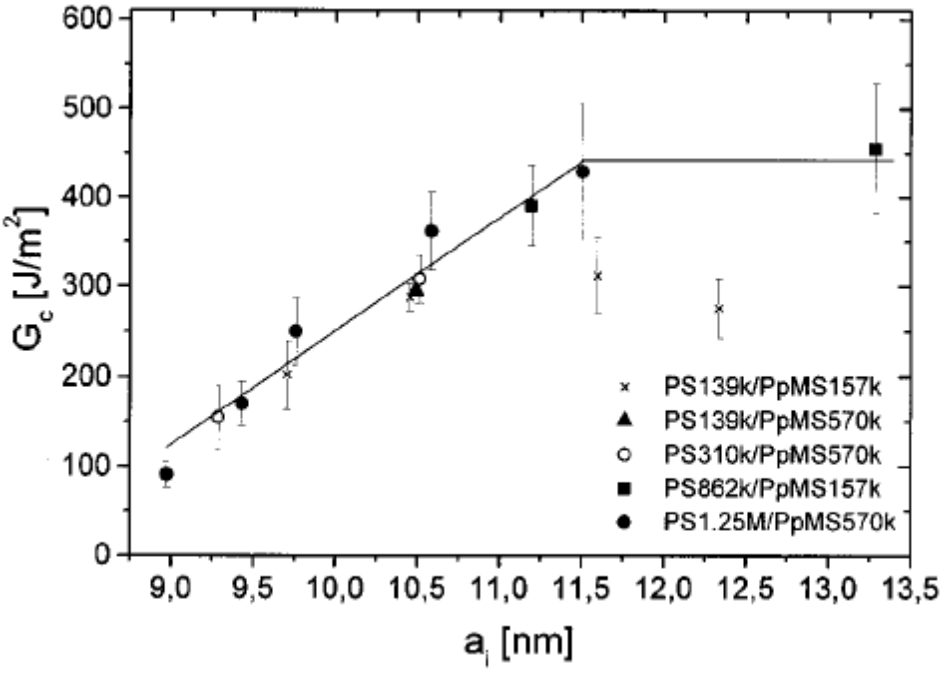

Figure 13. Adhesion toughness (G_c) of different samples of PS/PpMS plotted as a function of the interfacial width (a_i). The solid line is drawn as a guide to the eye[2].

We next move to the adhesion strength of the adsorbed layers. As summarized in Table 1, we found that the bottom 20kDa PEO interfacial sublayer (h = 8 nm), which are composed of loosely adsorbed chains and flattened chains, is still adhesive against the 200 nm-thick PEO films. This is consistent with previous reports that annealed spin-cast films with the thickness closed to R_g (For

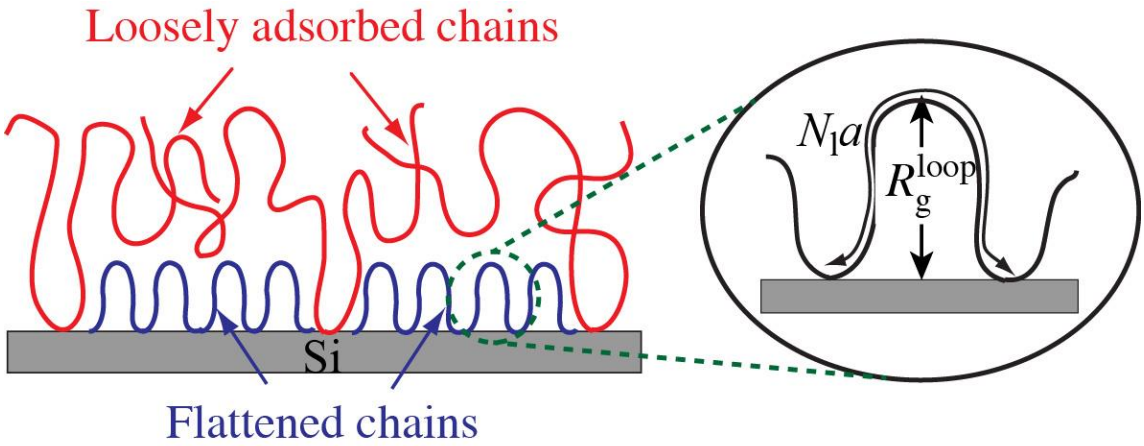

Figure 14. The sketch image of the chain structure of interfacial layer (left) and each loop of the flattened chains (right).

20kDa PEO, R_g=6.26 nm) have many solid-segment contacts, resulting in "Guiselin brushes"[94] (i.e., irreversibly adsorbed polymer layers). In contrast, we found the complete lack of adhesion between the PEO flattened layer (2.5 nm in thickness) composed of 20kPEO and the 200 nm-thick PEO films. As shown in Fig. 15, the surface of the flattened layer remained unchanged even after the adhesion experiment (Figs. 15a&c), demonstrating the anti-sticking property of the flattened layer. On the other hand, for the PEO adsorbed layer, the surface morphology after the adhesion experiment (Fig. 15d) was totally different from that before the adhesion experiment where finger-like seaweed flat-on lamellar structures[95],is clearly observed. In addition, we confirmed that the PEO flattened layer and interfacial sublayers used in this study have the same surface tension as a thick PEO film based on liquid contact angle measurements. Hence, we hypothesize that the anti-sticking property of the flattened layer is originated from the lack of chain entanglement between the flattened chains and the free chains in the overlayer. This can be rationalized by the size of the loop[96] or the actual tube diameter of the flattened chains that is not large enough to form a stable entanglement with the free chains, as depicted in the Fig. 3. Supposing that each loop of the flattened chains is composed of N_l segments (the right cartoon of Fig. 13), the size of loop can be approximated to be R_g of the loop (R_g^{loop})[96]. Based on the critical molecular weight for entanglements ($N_e \cong 40$ for PEO[88]), the critical size of R_g for PEO ($R_{g,c}$) is estimated to be $R_{g,c} \approx$ 1.9 nm (with a = 0.72 nm. Therefore, the loop size of the flattened chains (i.e., the thickness of the flattened layer (2.5 nm) is comparable to $R_{g,c}$: this would prevent entanglements between the flattened chains and free chains. On the other hand, once the loop sizes of the loosely adsorbed chains are larger than $R_{g,c}$, entanglements between the loosely adsorbed chains and the free polymer chains in the overlayer can be formed,[97, 98], resulting in the enhanced adhesion strength compared to the flattened chains used here.

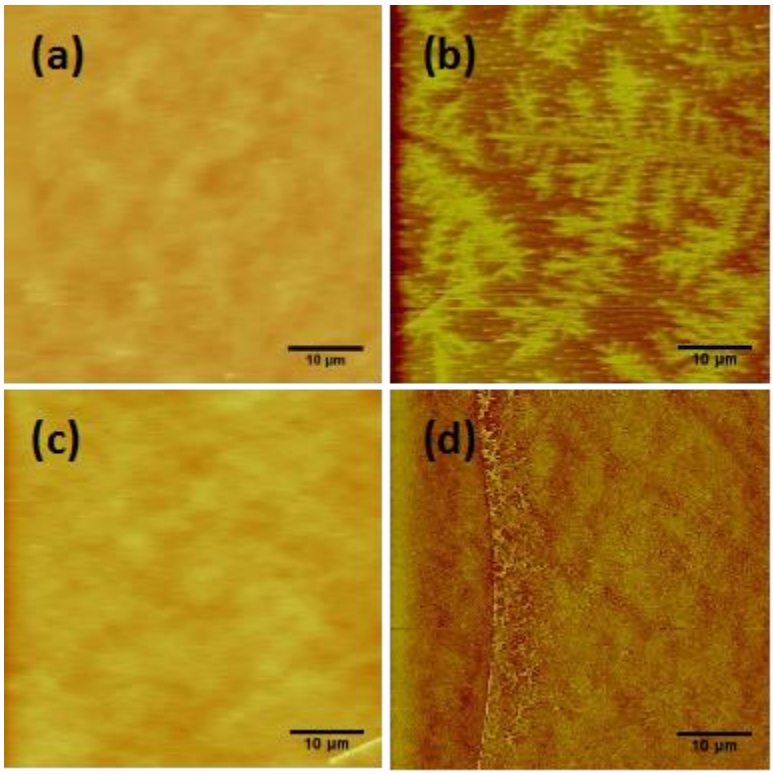

Figure 15. AFM images of thin films with different structure, PEO flattened layer (a,c), PEO interfacial layer (b,d), before adhesion experiments (a,b) and after adhesion for 24 hours (c,d).

Further adhesion experiments were performed with the PS flattened layers as well as the interfacial sublayers and the results are tabulated in Table 1. Hence, we can conclude that the flattened layers show the anti-sticking property regardless of a choice of polymers, while the interfacial sublayers are still adhesive. Interestingly, the critical normal stress of the interfacial sublayers is independent of M_w, while the thicknesses of the interfacial sublayers increase with increasing M_w. In addition, similar behavior was previously reported by other groups[2,99,100]. In their adhesion experiments for polystyrene-poly(2-vinylpyridine) reinforced with block polymer, the fracture toughness become independent of the molecular weight of the block when its molecular weight is higher than 5-6 M_e (for PVP, M_e=17,000) [99]. Besides, Wool al et[100] show that for pure PS, when the molecular weight is higher than $10M_e$, the fracture toughness become independent of the molecular weight. In addition, Schnell and co-workers[2] showed that the fracture toughness is independent when the molecular weight is higher than $8M_e$. Here in our experiment, the molecular weight of PS we used range from $7M_e$ to $40M_e$ (M_e for PS is 16,000). Thus, it may be reasonable to apply the same reason to our results: in this molecular weight region, molecular

event responsible for the failure is exclusively chain scission so that the fracture toughness is predicted to be molecular weight independent. It should be noted that the previous neutron reflectivity results showed that the interfacial width of the PS (650kDa) increased up to only 8.6 ± 0.3 nm even after 24 h annealing at 150 ℃[41].

We also investigated the surface morphology of the flattened layers and interfacial sublayers after the adhesion experiments. Fig. 16 shows the AFM results of the PS (Mw=100kDa) flattened

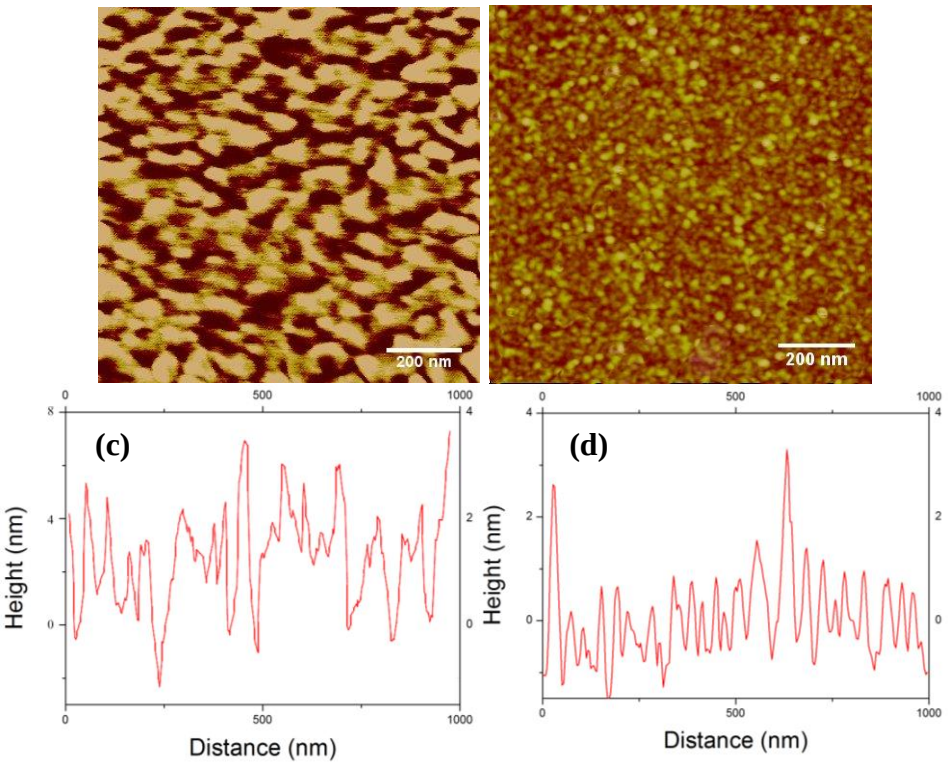

Figure 16. AFM images of the PS (Mw=100kDa) flattened layers annealed for 24 hours (a) and 11 days (b) and their height profile (c and d, respectively) after the adhesion experiments. The top layer thickness was 200 nm.

layer and interfacial sublayer after the adhesion experiments with the top PS layer (Mw=100kDa, the thickness was 200nm). From the image we can still see the nano-textures of the flattened layer even after the adhesion experiment for 24 h, which are in good agreement with the result before the adhesion experiments[96, 101], indicating that the morphology of the flattened layer remained unaffected. On the other hand, with 11 days annealing, the surface of the flattened layer now covers homogenously and becomes smoother (Fig. 16c and Fig. 16d). Our hypothesis is that, when the

temperature is above T_g, free unadsorbed chains from the top layer adsorb on the substrate, occupying the empty area of the flattened layer (indicated in the darker region of Fig. 16a). This process is sluggish because the mobility of polymer chains near the substrate is low in the melts[96, 101]. Thus, 24 hours may not be long enough for the unadsorbed chains to adsorb on the substrate strongly and be peeled off easily from the bottom substrate after the adhesion experiment. On the other hand, after 11 days, the free chains adsorbed on the substrate and form many solid-segment contacts, resulting in the stable flattened chains on the substrate. As a result, the thickness of bottom layer didn't change after 11 days adhesion (~2.5nm).

	Flattened layer (2.5 nm thick)	Interfacial sublayer (5-8 nm thick)
PEO(20kDa)	No adhesion	0.01519 MPa
PS(100kDa)	No adhesion	0.09034 MPa (4.5nm)
PS(221kDa)	No adhesion	0.10613 MPa (7nm)
PS(650kDa)	No adhesion	0.09212 MPa (10nm)

Table 1. Adhesion strength for the PEO and PS flattened layer or interfacial layer

Chapter 4 Conclusion and Future work

In summary, our experiments revealed the anomalous interaction between the adsorbed or flattened chains and the free chains composed of chemically identical polymers. We found that the equilibrium flattened layers do not show any mechanical adhesion property with the free polymer melts due to the lack of effective entanglement at the flattened chain – free chain interface. Such lack of entanglement is likely due to the denser, extremely contracted chain conformation of flattened chains on solid surface which prevents the flattened chains to connect with the free polymers. Moreover, this reduced chain entanglement density near the solid surface can propagate with a distance of at least 15 nm into the film interior, leading to a gradient of adhesion strength of thin polymer films as a function of distance from the solid interface. We also found that the non-sticky flattened layer has a profound impact on the recrystallization process of free chains from the melt: the crystalline structure and preferential lamellae orientation could be altered due to the unfavorable interaction between the flattened chains and free chains. Aside from the lack of chain entanglement at the interface, the failure of forming stable loosely adsorbed chains and negative excessive interfacial entropy between the flattened chains and free chains would also be other two responsible factors for such unfavorable interaction. These unique features of flattened layers not only improved our understanding of the polymer-polymer interaction near solid interfaces, but also shed new light on controlling and manipulating the mechanical adhesive and crystallization behavior of polymers near solids.

Next, I propose to elucidate the effects of the chain conformations of the connector molecules (a mixture of tails and loops[13, 102]) on the adhesive property. Using numerical self-consistent field treatment, Shull calculated the free energy of polymeric melts on monodisperse tails, monodisperse loops, and a polydisperse mixture of tails and loops[14]. He concluded that a polymer film on a polydisperse grafted layer can easily eliminate any tendency to give wetting autophobicity, while loops themselves contribute more than tails to the dewetting tendency[54]. In contrast, Dadmun and co-workers prepared a series of ditelechelic PS to form loops on solids and showed that the formation of the loops provides structures with which free polymer chains can entangle effectively, thereby improving the film stability on top of the loops[103-105]. Thus, comprehensive understanding of the roles of the nanoscale chain conformations at the polymer-solid interface in relation to film wettability/adhesive properties remains unresolved. To distinguish the roles of the tails and loops in the adsorbed chains, we propose to use monotelechelic (singly-bound) and ditelechelic (doubly-bound) polymers that will be grafted to Si substrates to

form tails (the singly-bound chains) or a majority of loops (the doubly-bound chains). We are currently using commercially available end-functionalized PS, monohydroxy-terminated PS (PS-OH, M_w=100kDa) and dicarboxy-terminated PS (COOH-PS-COOH, M_w=25kDa) as initial systems. For the brush film, we followed Tsui and co-worker's procedure[106]: piranha solution cleaned Si wafers were treated by a UV/ozone cleaner (UVOCS Inc.) for 30 min. XR results clarified that the resultant surface was covered with a homogenous 2.5 nm thick oxide layer. A toluene solution of the brush polymer was then spin-cast on the substrate and the spin-cast films were annealed at 150 ℃ for 24h. The unreacted polymer chains were rinsed off by thorough toluene leaching. We confirmed that the surface of the brush film was reasonably homogenous based on AFM experiments. For the doubly-bound polymer, we also used the UV ozone-treated Si substrate ("SiOx/Si" with a 2.5 nm thick SiOx layer). To promote the tethering of the dicarboxy-terminated PS chains, we adopted a Fischer esterification process (i.e., the esterification of a carboxylic acid by heating it with an alcohol in the presence of a strong acid (H_2SO_4) as the catalyst). The polymer solution with the acid was spread onto the surface of the SiOx/Si completely and was allowed to dry in air. The samples were then moved to a vacuum oven where they were annealed at 150 ℃ for 5 days. After this, the sample was rinsed with toluene to remove the unreacted polymer chains. Based on ellipsometry and AFM experiments, we found the final thickness of the loops to be 3.2 nm covered homogenously on the Si substrate. In order to determine the number of unreacted carboxylic acid end groups, a titration was performed on the annealed samples. Adding dilute NaOH (aq.) until the endpoint allowed for the moles of free carboxylic acid end groups on the substrate to be calculated. The result showed that about 65% of the carboxylic acid groups were bound to the substrate, forming loops upon adsorption on the Si substrate. This bound fraction is higher than that (≈ 57%) of α,ω-difunctional thiol telechelic PS (M_w=24.6kDa) prepared on a gold substrate[107]. In order to further increase the number of the bound fraction, we will use lower M_w ditelechelic PS, as Patton and co-workers demonstrated[107]. These chemically grafted tails and loops will be characterized by using XR and AFM. The brush and loop films will then be pressed together with an upper bulk PS film and subject to the proposed adhesion experiments. The results will be further compared with the adhesion force of end-grafted polymer brushes or ditelechelic polymer loops prepared on solids, shedding light on the roles of the tails and loops in the adhesion properties of the adsorbed chains.

References

1. Kausch, H. H.; Tirrell, M. *Annual Review of Materials Science* **1989,** 19, (1), 341-377.
2. Schnell, R.; Stamm, M.; Creton, C. *Macromolecules* **1998,** 31, (7), 2284-2292.
3. Burattini, S.; Greenland, B. W.; Chappell, D.; Colquhoun, H. M.; Hayes, W. *Chemical Society Reviews* **2010,** 39, (6), 1973-1985.
4. Richardson, H.; Carelli, C.; Keddie, J. L.; Sferrazza, M. *Eur. Phys. J. E* **2003,** 12, (3), 437-440.
5. Reiter, G.; Hamieh, M.; Damman, P.; Sclavons, S.; Gabriele, S.; Vilmin, T.; Raphael, E. *Nat. Mater.* **2005,** 4, (10), 754-758.
6. Damman, P.; Gabriele, S.; Coppee, S.; Desprez, S.; Villers, D.; Vilmin, T.; Raphael, E.; Hamieh, M.; Al Akhrass, S.; Reiter, G. *Phys. Rev. Lett.* **2007,** 99, (3), 4.
7. Thomas, K. R.; Chenneviere, A.; Reiter, G.; Steiner, U. *Phys. Rev. E* **2011,** 83, 021804.
8. Barbero, D. R.; Steiner, U. *Phys. Rev. Lett.* **2009,** 102, (24), 248303.
9. Chung, J. Y.; Chastek, T. Q.; Fasolka, M. J.; Ro, H. W.; Stafford, C. M. *ACS Nano* **2009,** 3, (4), 844-852.
10. Fujii, Y.; Yang, Z. H.; Leach, J.; Atarashi, H.; Tanaka, K.; Tsui, O. K. C. *Macromolecules* **2009,** 42, (19), 7418-7422.
11. Fleer, G. J.; Cohen Stuart, M. A.; Scheutjens, J. M. H. M.; Cosgrove, T.; Vincent, B., *Polymers at Interfaces*. Chapman and Hall: London, 1993.
12. Schuetjens, M. H. M.; Fleer, G. J. *J. Phys. Chem.* **1980,** 84, 178-190.
13. Guiselin, O. *Europhys. Lett.* **1992,** 17, (3), 225-230.
14. Shull, K. R. *Macromolecules* **1996,** 29, 8487-8491.
15. Durning, C. J.; O'Shaughnessy, B.; Sawhney, U.; Nguyen, D.; Majewski, J.; Smith, G. S. *Macromolecules* **1999,** 32, (20), 6772-6781.
16. Napolitano, S.; Wubbenhorst, M. *J. Phys. Chem. B* **2007,** 111, 9197-9199.
17. Napolitano, S.; Prevosto, D.; Lucchesi, M.; Pingue, P.; D'Acunto, M.; Rolla, P. *Langmuir* **2007,** 23, 2103-2109.
18. Napolitano, S.; Lupascu, V.; Wubbenhorst, M. *Macromolecules* **2008,** 41, 1061-1063.
19. Rotella, C.; Napolitano, S.; De Cremer, L.; Koeckelberghs, G.; Wubbenhorst, M. *Macromolecules* **2010,** 43, 8686-8691.
20. Napolitano, S.; Rotella, C.; Wubbenhorst, M. *Macromol. Rapid Commun.* **2011,** 32, 844-848.
21. Napolitano, S.; Wubbenhorst, M. *Nat. Commun.* **2011,** 2, 260-266.
22. Asada, M.; Jiang, N.; Sendogdular, L.; Gin, P.; Wang, Y.; Endoh, M. K.; Koga, T.; Fukuto, M.; Schultz, D.; Lee, M.; Li, X.; Wang, J.; Kikuchi, M.; Takahara, A. *Macromolecules* **2012,** 45, 7098-7106.
23. Koga, T.; Naisheng, J.; Gin, P.; Endoh, M.; Narayanan, S.; Lurio, L.; Sinha, S. K. *Phys. Rev. Lett.* **2011,** 107, 225901.
24. Gin, P.; Jiang, N. S.; Liang, C.; Taniguchi, T.; Akgun, B.; Satija, S. K.; Endoh, M. K.; Koga, T. *Phys. Rev. Lett.* **2012,** 109, (26), 265501.
25. Jiang, N. S.; Shang, J.; Di, X. Y.; Endoh, M. K.; Koga, T. *Macromolecules* **2014,** 47, (8), 2682-2689.
26. Villars, D. S. *J. Polym. Sci.* **1956,** 21, 257-271.
27. Medalia, A. I. *J. Colloid Interface Sci.* **1970,** 32, 115.
28. Blow, C. M. *Polymer* **1973,** 14, 309.

29. Dannenberg, E. M. *Rubber Chem. Technol.* **1986,** 59, 512.
30. Kenny, J. C.; McBrietry, V. J.; Rigbi, Z.; Douglass, D. C. *Macromolecules* **1991,** 24, 436.
31. Karasek, L.; Sumita, M. *J. Mater. Sci.* **1996,** 31, (2), 281-289.
32. Harton, S. E.; Kumar, S. K.; Yang, H. C.; Koga, T.; Hicks, K.; Lee, E.; Mijovic, J.; Liu, M.; Vallery, R. S.; Gidley, D. W. *Macromolecules* **2010,** 43, (7), 3415-3421.
33. Jouault, N.; Moll, J. F.; Meng, D.; Windsor, K.; Ramcharan, S.; Kearney, C.; Kumar, S. K. *ACS Macro Lett.* **2013,** 2, (5), 371-374.
34. Jiang, N.; Endoh, M. K.; Koga, T.; Masui, T.; Kishimoto, H.; Nagao, M.; Satija, S. K.; Taniguchi, T. *ACS Macro Lett.* **2015,** 4, 838-842.
35. Farago, B.; Monkenbusch, M.; Richter, D.; Huang, J. S.; Fetters, L. J.; Gast, A. P. *Phys. Rev. Lett.* **1993,** 71, 1015-1018.
36. Jiang, N.; Endoh, M. K.; Koga, T., Structures and Dynamics of Adsorbed Polymer Nanolayers on Planar Solid. In *Non-Equilibrium Phenomena in Confined Soft Matter*, Napolitano, S., Ed. Springer: 2015; pp 129-160.
37. Shin, K.; Hu, X.; Zheng, X.; Rafailovich, M. H.; Sokolov, J.; Zaitsev, V.; Schwarz, S. A. *Macromolecules* **2001,** 34, 4993-4998.
38. Seeck, O. H.; Kaendler, I. D.; Tolan, M.; Shin, K.; Rafailovich, M. H.; Sokolov, J.; Kolb, R. *Appl. Phys. Lett.* **2000,** 76, (19), 2713-2715.
39. Koga, T.; Seo, Y. S.; Jerome, J.; Ge, S.; Rafailovich, M. H.; Sokolov, J. C.; Chu, B.; Seeck, O. H.; Tolan, M.; Kolb, R. *Appl. Phys. Lett.* **2003,** 83, 4309-4311.
40. Gin, P.; Asada, M.; Endoh, M. K.; Gedelian, C.; Lu, T. M.; Koga, T. *Appl. Phys. Lett.* **2009,** 94.
41. Jiang, N.; Wang, J.; Di, X.; Cheung, J.; Zeng, W.; Endoh, M. K.; Koga, T.; Satija, S. K. *Submitted for publication.*
42. Linse, P.; Källrot, N. *Macromolecules* **2010,** 43, (4), 2054-2068.
43. O'Shaughnessy, B.; Vavylonis, D. *Eur. Phys. J. E* **2003,** 11, (3), 213-230.
44. O'Shaughnessy, B.; Vavylonis, D. *J. Phys. Condens. Matter.* **2005,** 17, (2), R63-R99.
45. Källrot, N.; Linse, P. *Macromolecules* **2007,** 40, (13), 4669-4679.
46. Asada, M.; Jiang, N.; Sendogdular, L.; Sokolov, J.; Endoh, M. K.; Koga, T.; M.Fukuto; Yang, L.; Akgun, B.; Dimitriou, M.; Satija, S. K. *Soft Matter* **2014,** 10, 6392-6403.
47. Muller-Buschbaum, P. *Eur. Phys. J. E* **2003,** 12, 443-448.
48. Redon, C.; Brochard-Wyart, F.; Rondelez, F. *Phys. Rev. Lett.* **1991,** 6, 715-718.
49. Debrégeas, G.; Martin, P.; Brochard-Wyart, F. *Phys. Rev. Lett.* **1995,** 75, 3886-3889.
50. Muller-Buschbaum, P.; Vanhoorne, P.; Scheumann, V.; Stamm, M. *Europhys. Lett.* **1997,** 40, (6), 655-660.
51. Muller, M.; MacDowell, L. G.; Muller-Buschbaum, P.; Wunnike, O.; Stamm, M. *J. Chem. Phys.* **2001,** 115, (21), 9960-9969.
52. Hare, E. F.; Zisman, W. A. *J. Phys. Chem.* **1955,** 59, 335-340.
53. Leibler, L.; Ajdari, A.; Mourran, A.; Coulon, G.; Chatenay, D., Wetting of Grafted Polymer Surfaces by Compatible Chains. In *Ordering in Macromolecular Systems*, Teramoto, A.; Kobayashi, M.; Norisuye, T., Eds. Springer: Berlin, 1994; pp 301-311.
54. Shull, K. R. *Faraday Discuss.* **1994,** 98, 203-217.
55. Reiter, G.; Auroy, P.; Auvray, L. *Macromolecules* **1996,** 29, (6), 2150-2157.
56. Ferreira, P. G.; Ajdari, A.; Leibler, L. *Macromolecules* **1998,** 31, 3994-4003.
57. Reiter, G.; Khanna, R. *Phys. Rev. Lett.* **2000,** 85, (26), 5599-5602.
58. Zhang, X.; Lee, F. K.; Tsui, O. K. C. *Macromolecules* **2008,** 41, 8148-8151.

59. Housmans, C.; Sferrazza, M.; Napolitano, S. *Macromolecules* **2014,** 47, (10), 3390-3393.
60. Brown, H. *Annual Review of Materials Science* **1991,** 21, (1), 463-489.
61. Doi, M.; Edwards, S. F., *The theory of polymer dynamics*. oxford university press: 1988; Vol. 73.
62. Pierce, F.; Perahia, D.; Grest, G. *EPL (Europhysics Letters)* **2011,** 95, (4), 46001.
63. Kunz, K.; Stamm, M. *Macromolecules* **1996,** 29, (7), 2548-2554.
64. Reiter, G.; Steiner, U. *Journal de Physique II* **1991,** 1, (6), 659-671.
65. Felcher, G. P.; Karim, A.; Russell, T. P. *Journal of Non-Crystalline Solids* **1991,** 131, 703-708.
66. Prager, S.; Tirrell, M. *The journal of chemical physics* **1981,** 75, (10), 5194-5198.
67. Tirrell, M.; Adolf, D.; Prager, S., Orientation and motion at a polymer-polymer interface: Interdiffusion of fluorescent-labelled macromolecules. In *Orienting Polymers*, Springer: 1984; pp 37-45.
68. Mikos, A. G.; Peppas, N. A. *The Journal of chemical physics* **1988,** 88, (2), 1337-1342.
69. Jud, K.; Kausch, H.; Williams, J. *Journal of Materials Science* **1981,** 16, (1), 204-210.
70. Russell, T.; Deline, V.; Dozier, W.; Felcher, G.; Agrawal, G.; Wool, R.; Mays, J. *Nature* **1993,** 365, (6443), 235-237.
71. Washiyama, J.; Kramer, E. J.; Hui, C. Y. *Macromolecules* **1993,** 26, (11), 2928-2934.
72. Schnell, R.; Stamm, M.; Creton, C. *Macromolecules* **1999,** 32, (10), 3420-3425.
73. Ge, T.; Pierce, F.; Perahia, D.; Grest, G. S.; Robbins, M. O. *arXiv preprint arXiv:1211.6796* **2012**.
74. Ge, T.; Grest, G. S.; Robbins, M. O. *Macromolecules* **2014,** 47, (19), 6982-6989.
75. Davis, C. S.; Lemoine, F.; Darnige, T.; Martina, D.; Creton, C.; Lindner, A. *Langmuir* **2014,** 30, (35), 10626-10636.
76. Sha, Y.; Hui, C. Y.; Kramer, E. J.; Hahn, S. F.; Berglund, C. A. *Macromolecules* **1996,** 29, (13), 4728-4736.
77. Frank, B.; Gast, A. P.; Russell, T. P.; Brown, H. R.; Hawker, C. *Macromolecules* **1996,** 29, (20), 6531-6534.
78. Lin, E. K.; Wu, W.-l.; Satija, S. K. *Macromolecules* **1997,** 30, (23), 7224-7231.
79. Zheng, X.; Rafailovich, M.; Sokolov, J.; Strzhemechny, Y.; Schwarz, S.; Sauer, B.; Rubinstein, M. *Physical Review Letters* **1997,** 79, (2), 241.
80. Zheng, X.; Sauer, B.; Van Alsten, J.; Schwarz, S.; Rafailovich, M.; Sokolov, J.; Rubinstein, M. *Physical Review Letters* **1995,** 74, (3), 407.
81. Raphael, E.; De Gennes, P. G. *J. Phys. Chem.* **1992,** 96, 4002-4007.
82. Jones, R. A.; Richards, R. W., *Polymers at Surfaces and Interfaces*. Chambridge University Press: 1999.
83. Leger, L.; Creton, C. *Phil. Trans. R. Soc. A* **2008,** 366, 1425-1442.
84. Graessley, W. W. *J. Polym. Sci. Part B. Polym. Phys.* **1980,** 18, 27-34.
85. Julia Nase, O. R., Costantino Creton, and Anke Lindner. *The European Physical Journal E* **2013,** 36, (9), 1-10.
86. J. E. Ritter, T. J. L., L. Rosenfeld, and M. R. Lim. *Journal of Applied Physics* **1989,** 66, (8), 3626-3634.
87. Peppas, N. A.; Wu, J.; von Meerwall, E. D. *Macromolecules* **1994,** 27, (20), 5626-5638.
88. Fetters, L.; Lohse, D.; Colby, R., Chain dimensions and entanglement spacings. In *Physical properties of polymers handbook*, Springer: 2007; pp 447-454.
89. Cole, P. J.; Cook, R. F.; Macosko, C. W. *Macromolecules* **2003,** 36, (8), 2808-2815.

90. da Silva, L. F. M., *Handbook of adhesion technology: with 97 tables*. Springer Science & Business Media: 2011.
91. Ge, T.; Pierce, F.; Perahia, D.; Grest, G. S.; Robbins, M. O. *Physical Review Letters* **2013,** 110, (9), 098301.
92. Chunhua, L.; Hyunjung, K.; Jun, J.; Clive, L.; Tadanori, K.; Laurence, L.; Steve, S.; Suresh, N.; Heeju, L.; Young Joo, L.; Zhang, J.; Sunil, S.; Rafailovich, M. H.; J. C. Sokolov. *EPL (Europhysics Letters)* **2006,** 73, (6), 899.
93. Brown, H. R. *Macromolecules* **2001,** 34, (11), 3720-3724.
94. Guiselin, O. *EPL (Europhysics Letters)* **1992,** 17, (3), 225.
95. Asada, M.; Jiang, N.; Sendogdular, L.; Sokolov, J.; Endoh, M. K.; Koga, T.; Fukuto, M.; Yang, L.; Akgun, B.; Dimitriou, M. *Soft matter* **2014,** 10, (34), 6392-6403.
96. Gin, P.; Jiang, N.; Liang, C.; Taniguchi, T.; Akgun, B.; Satija, S. K.; Endoh, M. K.; Koga, T. *Phys Rev Lett* **2012,** 109, (26), 265501.
97. Huang, Z.; Ji, H.; Mays, J. W.; Dadmun, M. D. *Macromolecules* **2008,** 41, (3), 1009-1018.
98. Patton, D.; Knoll, W.; Advincula, R. C. *Macromol Chem Phys* **2011,** 212, (5), 485-497.
99. Creton, C.; Kramer, E. J.; Hui, C. Y.; Brown, H. R. *Macromolecules* **1992,** 25, (12), 3075-3088.
100. Wool, R. P., *Polymer interfaces: structure and strength*. Hanser: 1995.
101. Jiang, N.; Shang, J.; Di, X.; Endoh, M. K.; Koga, T. *Macromolecules* **2014,** 47, (8), 2682-2689.
102. Fujii, Y.; Yang, Z.; Clough, A.; Tsui, O. K. C. *Macromolecules* **2010,** 43, 4310-4313.
103. Dadmun, M. *Macromolecules* **1996,** 29, (11), 3868-3874.
104. Eastwood, E. A.; Dadmun, M. D. *Polymer* **2002,** 43, (25), 6707-6717.
105. Eastwood, E. A.; Dadmun, M. D. *Macromolecules* **2002,** 35, (13), 5069-5077.
106. Zhang, X.; Lee, F. K.; Tsui, O. K. C. *Macromolecules* **2008,** 41, 8148-8151.
107. Patton, D.; Knoll, W.; Advincula, R. C. *Macromol. Chem. Phys.* **2011,** 212, 485-497.